ORIGINAL ARTICLE

Unraveling the main issues of direct sample printing and sample cutting from a sheet of tensile test samples for characterization of Material Extrusion components

Francesco Lambiase[1] · Silvia Ilaria Scipioni[1] · Francesco Pace[1] · Alfonso Paoletti[1]

Abstract

This research investigates the influence of varied sample manufacturing strategies on the mechanical properties of Material Extrusion (MatExt) Additive Manufacturing components. Two procedures were investigated: direct sample printing and sample cutting from a sheet. The thickness of the samples was also varied to determine possible differences in the measurements performed. Through a comprehensive analysis involving mechanical testing, optical microscopy, and IR thermography during deposition, the study revealed significant implications of the manufacturing strategy on the thermal history and polymer chain entanglement. The results indicated that Young's modulus and the tensile strength produced through direct printing differed from that measured on the samples made through sample cutting. At the same time, the elongation at rupture was less influenced by the manufacturing strategy. The sample thickness also influenced the fracture strength; the thicker samples were characterized by a strength of 27.9 MPa, which was higher by 23% than that of the extracted samples.
The observed differences in mechanical behavior underscore the critical role of sample manufacturing strategy in determining the final mechanical properties of upright samples. Results shed light on the complex interplay between manufacturing protocols and component performance in MatExt applications.

Keywords Additive manufacturing · Material Extrusion · Mechanical characterization · Thermal history · Interlayer adhesion

1 Introduction

In the contemporary industrial landscape, advanced manufacturing processes have revolutionized the production of complex components, driving innovation and transforming traditional manufacturing methodologies. Among these cutting-edge techniques, additive manufacturing, also known as 3D printing, has emerged as a pivotal technology that facilitates the efficient and precise creation of intricate structures with unprecedented flexibility and customization [1–3]. This transformative capability has garnered widespread attention across diverse sectors, including aerospace, automotive, healthcare, and consumer goods industries, sparking a fundamental shift in how products are designed, developed, and fabricated [4–7]. Various factors, including advancements in material science, computational modeling, and process optimization, have fueled the rapid evolution of additive manufacturing technologies. Leveraging the principles of additive manufacturing, intricate designs [8] that were once deemed unfeasible or excessively costly to manufacture using conventional techniques are now being realized with greater ease and efficiency [9]. This fundamental shift has not only redefined the boundaries of design but has also accelerated the pace of innovation, enabling the realization of complex geometries, enhanced functional integration, and the production of lightweight, high-strength components with superior mechanical properties [10–12].

Within the realm of additive manufacturing, the Material Extrusion (MatExt) process, also widely known as Fused Filament Modeling (FDM) and Fused Filament Fabrication (FFF), has emerged as a prominent technique for fabricating intricate components with exceptional structural integrity and dimensional accuracy [13–15].

✉ Francesco Lambiase
  francesco.lambiase@univaq.it

1 Department of Industrial and Information Engineering and Economics (DIIIE), University of L'Aquila, Montelucco di Roio, 67100 L'Aquila, Italy

By utilizing a layer-by-layer deposition approach, MatExt technology enables the creation of robust components using a diverse range of thermoplastic materials, offering enhanced design flexibility and cost-effective production capabilities [16]. As the demand for lightweight, high-performance components continues to rise across various industries [17], the adoption of MatExt has become increasingly pervasive, with a pronounced emphasis on optimizing the mechanical properties and structural performance of the manufactured parts.

The multifaceted nature of MatExt technology underscores the importance of a comprehensive understanding of the intricate interplay between process parameters, material properties, and design considerations [18–20].

Successful implementation of MatExt necessitates a holistic approach that encompasses meticulous material selection, precise process parameter calibration, and the integration of advanced post-processing techniques to achieve the desired mechanical characteristics and dimensional accuracy [21]. This intricate interdependence between process variables and material behavior has prompted extensive research to elucidate the underlying mechanisms governing the structural performance and material properties of MatExt-produced components.

To enhance the mechanical properties and performance characteristics of MatExt components, an in-depth exploration of the intricate factors influencing the material behavior, interlayer adhesion, and structural integrity is imperative [22–24]. By delving into the complexities of the MatExt process, researchers and industry practitioners can gain valuable insights into the nuanced interactions between process parameters, thermal history, and microstructural evolution, thereby facilitating the development of robust frameworks for optimizing component design, material selection, and manufacturing protocols.

Moreover, the dynamic nature of additive manufacturing processes necessitates a comprehensive evaluation of the implications of varying manufacturing strategies on the final product quality, structural integrity, and mechanical behavior [20, 25].

By dissecting the influence of diverse sample manufacturing strategies on the measured mechanical properties, researchers can unravel the critical nuances that govern the material behavior and structural performance of MatExt components, paving the way for the formulation of advanced manufacturing protocols that cater to specific application requirements and performance benchmarks.

Many researchers investigated the influence of the process parameters on the tensile behavior of samples produced through the Material Extrusion process [26–30]. However, in many cases, tensile tests were not conducted along the sample growing direction but rather in the planar direction [31, 32]. It is well known that the tensile properties of these samples along the growing direction (z-direction) strongly affect the mechanical behavior of MatExt components since they

are prone to delamination [33–35]. Thus, when identifying optimal deposition conditions, the primary aspect should be to ensure strong adhesion between the consecutive layers.

Several studies have emphasized the intrinsic link between the thermal history and the mechanical properties of Material Extrusion Additive Manufacturing components [36–39]. This critical association arises from the level of intertwining among adjacent filaments, directly influencing interfilamentous adhesion. Understanding this interplay is vital for comprehensively deciphering the impact of process parameters on component mechanical performance and refining optimal processing conditions. Equally pivotal is the recognition that variations in component dimensions and geometries can substantially alter the thermal history, consequently affecting mechanical properties.

Existing research predominantly addresses the direct printing of samples, potentially introducing artifacts that skew mechanical behavior assessments. Lambiase and Scipioni [40] observed such discrepancies while investigating the influence of manufacturing strategies on the compressive mechanical behavior of MatExt-produced polylactide acid (PLA) components. Significant differences were discovered between directly printed samples and those cut from larger components. These alterations stem from multiple factors:

> Thermal history variance: the completion time for each layer is contingent on its dimensions, resulting in a lower interlayer time for directly printed samples compared to their larger counterparts.
> Edge effects: directly printed samples exhibit uneven filament distribution, which is particularly noticeable at the edges. This discrepancy arises from the lower hot end speed experienced at the edge due to deceleration and acceleration during directional changes.

Both types of defects exerted a considerable influence on the compressive behavior of the samples. The primary inquiries guiding this research are the following:

> Are directly printed samples adequate for characterizing the tensile mechanical behavior of MatExt components? To what extent, if any, do variations exist in the mechanical properties determined through direct sample printing versus cut samples when tested under tensile stress?

Given the close relationship between the thermal history and the entanglement of polymeric chains, it is reasonable to anticipate substantial disparities between directly printed samples manufactured at their final dimensions and those cut from larger printed structures to attain the desired final dimensions. This anticipation motivated a thorough comparative analysis of tensile samples. Specifically, we prepared tensile specimens oriented along the building direction

using direct printing and sample extraction (waterjet cutting) methodologies. Our investigation encompassed a comprehensive assessment of physical properties, including inner void dimensions, complemented by tensile tests to elucidate crucial mechanical properties such as elastic modulus and yield strength. Concurrently, thermal analysis during the sample printing process was conducted to elucidate the impact of sample dimensions on thermal history, offering insights into their physical and mechanical attributes.

2 Materials and methods

2.1 Materials and sample preparation

Polylactide acid (PLA), provided by RS PRO, was utilized for the study, boasting an initial diameter of 1.75 mm ± 0.02 mm. The samples were produced using a Creality Ender 6 commercial machine. Simplify 3D version 4.1.2 was used as slicing software. The critical deposition parameters, as listed in Table 1, significantly impact interlayer bonding behavior, surface roughness, and dimensional precision. Key factors such as nozzle temperature, layer thickness, building plate temperature, extrusion multiplier, infill percentage, and nozzle speed directly govern the thermal history, thereby influencing interlayer bonding and overall print quality.

The samples were manufactured according to ASTM D638 [41] standards.

Particularly, the samples were produced using different processes:

1) Direct printing: the samples were printed at the final dimension; thus, any further post-process was needed before characterization;
2) Sample extraction: the samples were cut through abrasive waterjet cutting. To this end, a box with side walls of 2.5 mm and 3 mm of thickness was printed. Then, the samples were cut from the box. To this end, the adoption

Table 1 Main deposition conditions

Process parameter	Value
Nozzle temperature (°C)	210
Building plate temperature (°C)	60
Hot-end speed (mm/min)	3000
Nozzle diameter (mm)	0.4
Extrusion width (mm)	0.5
Layer thickness (mm)	0.2
Infill percentage (%)	100
Infill strategy	Rectilinear
Number of external shells	1
Extrusion multiplier	100%

of waterjet cutting enabled the avoidance of any material modification since no heating was produced during the cutting operation.

Figure 1 presents a detailed schematic of the samples.

Additionally, six small-sized samples (designed according to ASTM D638 [41] Type V) were also produced using the extraction method to identify possible differences in terms of mechanical behavior. To this end, the samples were extracted from the same box with the same dimensions as that used for the production of Type I samples (80-mm width and 180-mm height) to preserve the thermal history.

The test matrix of the experimental campaign is summarized in Table 2.

2.2 Process monitoring

The mechanical properties of samples produced via the MatExt process are intricately influenced by material viscosity (during the extrusion), polymer chain entanglement, and possible crystallization of the material. As mentioned earlier, while maintaining all the process parameters constant, the geometry and dimensions of the component (sample) significantly impact the temperature history. Consequently, thermal analysis was performed to uncover how sample dimensions affect the thermal history of different manufacturing strategies. Additionally, the potential development of edge effects during the printing process, which could impact sample characteristics, was investigated. Thus, an infrared camera, the FLIR E60 model, was involved in the MatExt process for real-time temperature distribution monitoring. Following the methodology outlined in [40], the thermal camera was positioned adjacent to the specimen to record the thermal cycles occurring during printing, as depicted in Fig. 2. The acquisition frequency was set to the maximum available (30 Hz) to ensure high-quality data capture, considering the extended deposition time of up to 7 h for manufacturing the entire specimen. Subsequently, ResearchIR software was employed to analyze the thermal history. The thermal camera was securely mounted on the machine frame, enabling continuous temperature monitoring throughout the deposition process.

2.3 Sample characterization

The samples underwent geometrical characterization prior to mechanical testing to determine their densities. The dimensions were measured through microscopy analysis. This enabled us to determine the effective adhesion area, neglecting external defects.

Tensile tests were performed using a universal testing machine model C43.50 equipped with a 50-kN load cell. The tests were conducted at a traverse speed of 2 mm/min. During the tests, the strain of the sample was measured using an extensometer model 632.24F-50 by MTS. The tests were carried out until the samples
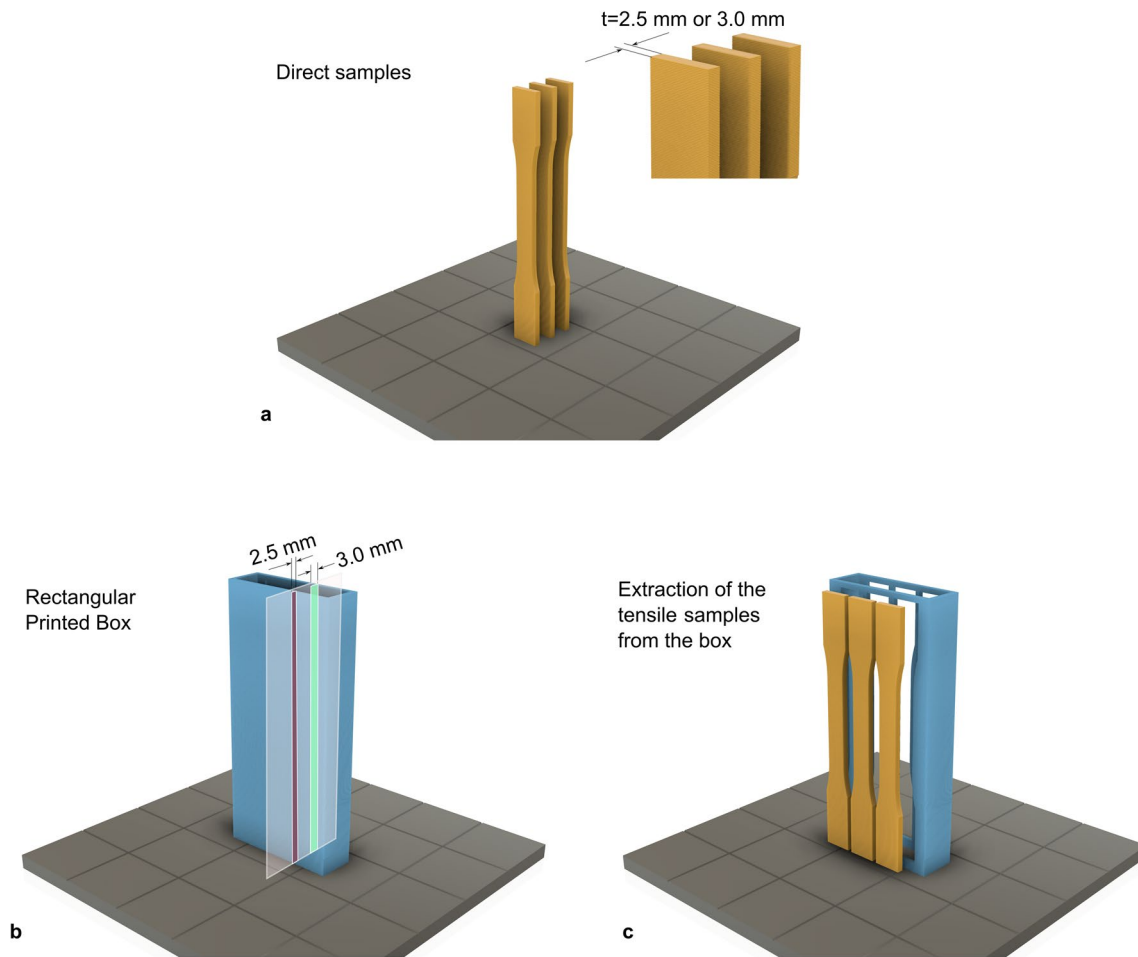
Fig. 1 Schematic of the sample produced using different approaches: **a** direct sample printing, **b** rectangular box printing, and **c** extraction (through abrasive waterjet cutting) of tensile samples from the rectangular box

Table 2 Test matrix summarizing the experimental conditions used for the experimental investigation

Condition	Sample geometry	Sample manufacturing	Thickness (mm)
I	ASTM D638 Type I	Direct sample printing	2.5
II	ASTM D638 Type I	Direct sample printing	3.0
III	ASTM D638 Type I	Plate printing and waterjet cutting	2.5
IV	ASTM D638 Type I	Plate printing and waterjet cutting	3.0
V	ASTM D638 Type V	Plate printing and waterjet cutting	3.0

were completely failed. A picture of the sample during the tensile test is presented in Fig. 3. Unfortunately, the extensometer was too large to be used in Type V samples. For these samples, only the fracture strength was determined.

Optical microscopy served as a valuable tool in understanding the material's morphology, both pre- and post-mechanical tests. To this end, a stereoscope model M205 by LEICA was used to determine the real dimension of the cross section, the surface morphology, and the analysis of the fracture surface.

3 Results

3.1 Mechanical behavior

After the tensile tests, the fracture developed in the middle of the samples, except for samples of Type V. In these samples, the fracture developed at the fillet just before the clamping area, as shown in Fig. 4.
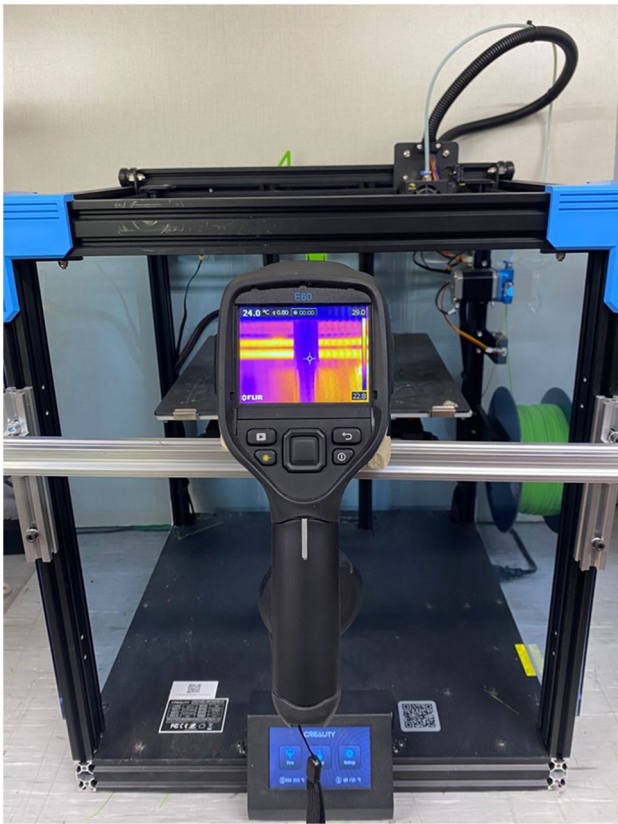
Fig. 2 Picture of the IR thermal measurement during the MatExt process

Fig. 3 Picture of the sample during the tensile test with **a** extensometer and **b** DIC equipment

Figure 5 depicts the stress-strain curves recorded during the tensile tests using different sample manufacturing protocols. For each sample manufacturing strategy and thickness, two curves were reported to check the repeatability. Type V samples were not reported since the dimension of the extensometer did not fit with the dimensions of these samples. Thus, for Type V samples, only the strength information was recorded.

All the curves showed an initial almost linear increase of stress pertaining to the elastic regime, followed by a peak load, which was followed by a plateau, indicating the onset of plastic strain. After the small plastic deformation, the load suddenly fell to zero, and brittle failure occurred.

The main mechanical characteristics were identified from the stress-strain curves, including Young's modulus, the elongation at rupture, and the peak strength. This enabled a better comparison among the samples produced with different protocols and thicknesses. For each sample, the average and the standard deviation were calculated. For samples of Type V, only the peak strength was calculated (since the tests were conducted without the extensometer). Figure 6a compares the Young's modulus of the samples. As can be inferred, the samples produced by direct printing exhibited a similar Young's modulus (with an average value of 2.51 GPa), irrespective of the thickness of the samples. On
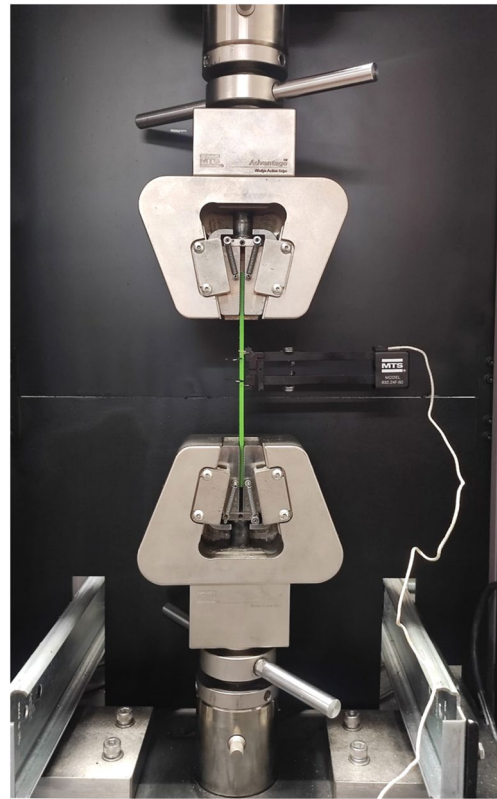
the other hand, the samples cut from the box had Young's modulus, which was influenced by the thickness of the wall: for samples of 2.5 mm (viz 3.0 mm) of thickness, Young's modulus was 2.4 GPa (viz. 2.8 GPa). This indicated that the elastic properties of the samples were influenced by the interlayer time and the thickness of the samples.

Figure 6b compares the peak strength of the samples: here, a more marked difference among the specimen manufacturing strategy is noticeable. Direct printed samples showed a peak strength of almost 31 MPa, which was higher than that of cut samples, which was 23 MPa (for cut samples with 2.5 mm of thickness) and 28 MPa (for samples with 3.0 mm of thickness). Finally, the samples cut from the box with Type V dimensions were characterized by even lower peak strength with a mean value of 21 MPa. This was due to the premature fracture of the samples in correspondence with the fillet's regions. Figure 6c indicates a lower influence of the manufacturing strategy and the thickness of the sample of the elongation at rupture e_{max}.

3.2 Fracture surface analysis

Optical microscopy of the fracture surfaces was performed to understand the influence of the sample manufacturing

Fig. 4 Pictures of samples produced according to ASTM D638 standards according to different types: **a** Type II and **b** Type V
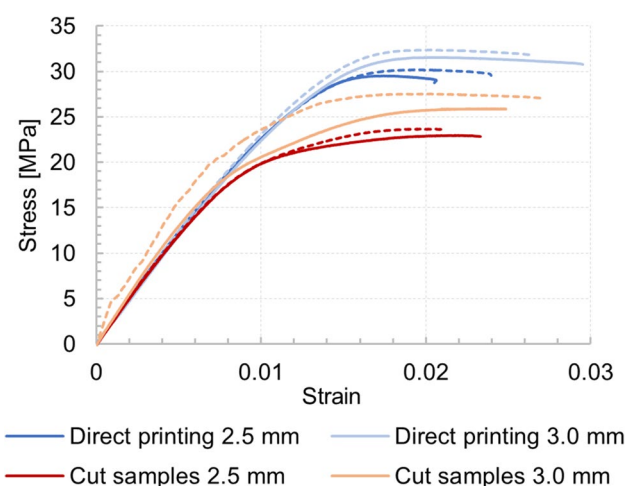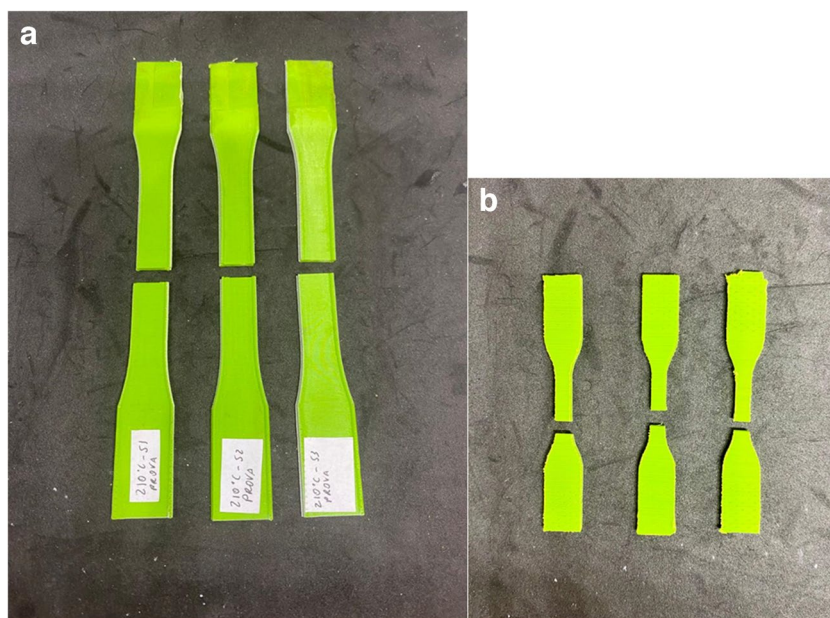

Fig. 5 Stress-strain curves of different samples produced with direct sample printing and cutting with two thicknesses

strategy on the failure modes. Two main failures were identified in the samples: intralayer fracture and delamination, as shown in Fig. 7. Intralayer fracture was observed on samples that showed the highest tensile strength. Herein, the adhesion between consecutive layers was so strong that a crack fractured some filaments (of the same layer), as shown in Fig. 7a. On the other hand, delamination (interlayer) involved the failure of the bonding between consecutive layers, as depicted in Fig. 7b. The onset of delamination indicates a weaker adhesion produced during the MatExt process as compared to intrafilamentary fracture. However, even in delaminated samples, the fracture surfaces were different: in some cases, the fracture surface was characterized

by irregular morphology, indicating higher interlayer adhesion, while in other regions, smoother surfaces were found, indicating lower adhesion.

Intralayer fracture was observed in directly printed samples (irrespective of the thickness) as well as in cut samples with thicker walls (3.0 mm of thickness). This further confirms how the manufacturing strategy and the thickness of the sample can influence the mechanical behavior and, more specifically, the fracture strength of components made by the MatExt process.

A higher magnification (SEM) image of intralayer fracture is reported in Fig. 8. From this picture, it is evident that strong adhesion arises between the layers.

The fracture surfaces analysis enabled to better identify some defects in the samples. Figure 9 shows the fracture surface of a sample of 3.0 mm of thickness made by direct printing. As can be inferred, the samples show some artifacts produced with direct printing. The layer entry region (LAYER START) and exit region (LAYER STOP) are distinguishable, and the higher amount of material deposited at the edges corresponds with the change in direction regions. Here, as reported in [40], the tool decelerates, stops, and then reverses in direction and accelerates again up to the prescribed printing speed. Hence, in correspondence with the edges, the high pressure of the material within the nozzle involves a higher amount of material being deposited, leading to an uneven deposition (edge effect). Although higher adhesion is observed in correspondence of the edges, this clearly alters the mechanical behavior exhibited by the directly printed samples, leading to superior mechanical behaviors compared to a larger component.

Fig. 6 Mechanical characteristics of the samples produced using different manufacturing strategies
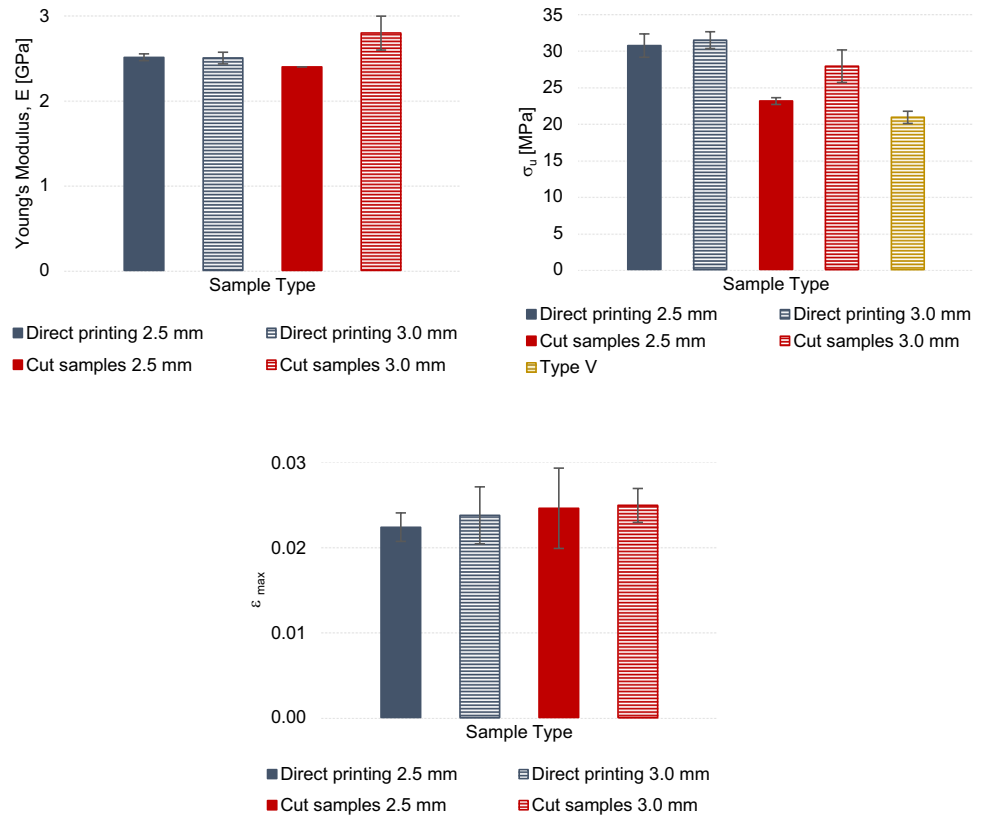

Fig. 7 Different fracture modes in samples of 2.5 mm of thickness made by **a** direct printing (intralayer fracture) and **b** cutting from larger component (interlayer fracture)
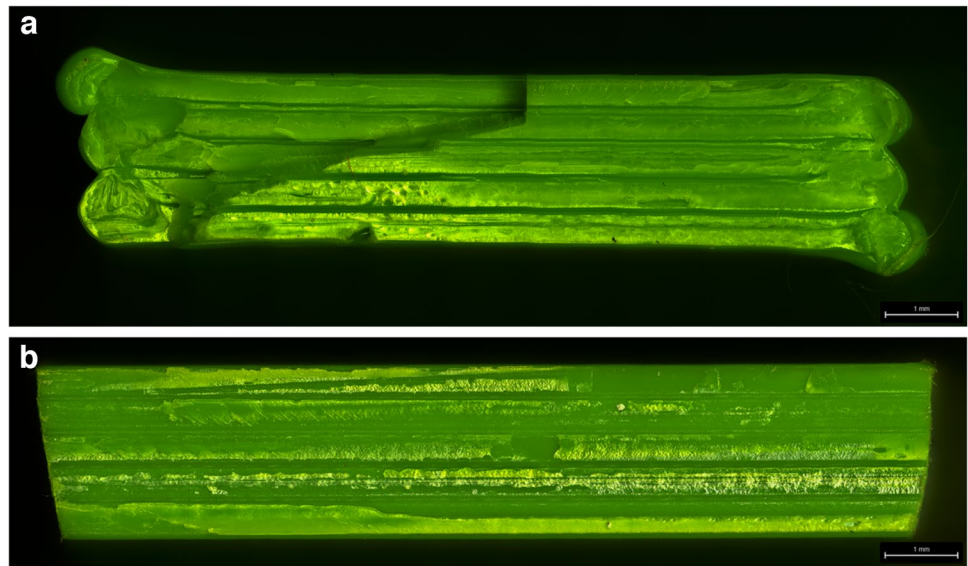

Figure 10 compares the fracture surfaces of two samples cut from the box, which have 2.5- and 3.0-mm thicknesses, respectively. Even though both the fracture surfaces reveal a strong interlayer adhesion, the fracture surface of the thicker sample shows intralayer fracture. This is indicative of an even higher adhesion, in agreement with the measurements reported in Fig. 6b. The samples were extracted from two different sides of the same box. Consequently, they shared the same interlayer time (29.9 s). This indicates a high sensitivity of the mechanical behavior to the thickness of the sample. Such an effect was addressed to the higher thermal inertia of thicker samples as compared to the thinner ones (2.5 mm).

A cross-sectional analysis was performed on samples produced through direct printing and cutting from the plate, as depicted in Fig. 11. The cross sections show the

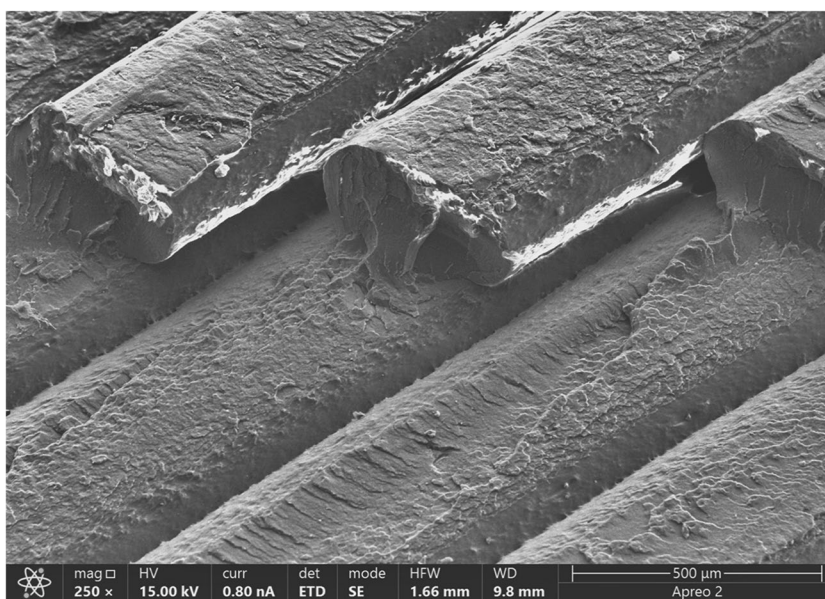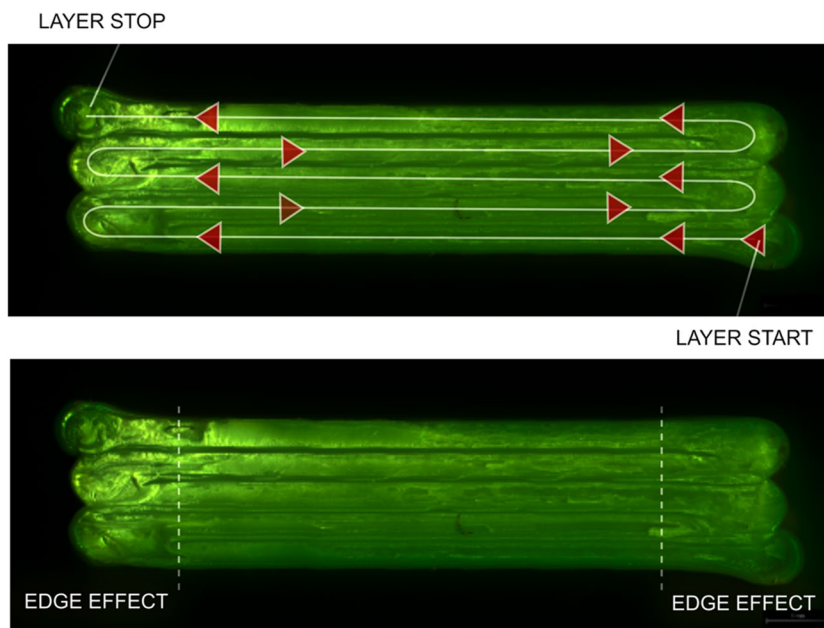**Fig. 8** SEM image of the intralayer fracture of a specimen made by direct printing

Fig. 9 Artifacts affecting the interlayer deposition in directly printed samples

interfilamentous porosities that develop between adjacent filaments. As can be observed, the porosities in the directly printed samples are larger than those observed in the cut samples, as also confirmed by the histograms reported in Fig. 12.

3.3 Thermal analysis

The temperature of the sample during the printing process was monitored with the aim of determining how the different sample dimensions affect the thermal history and, consequently, the polymer chain entanglement that determined the fracture strength of the samples. Figure 13 compares the IR maps recorded during the deposition of directly printed samples and a box (from which the samples will be cut).

The temperature maps indicate a sudden cooling of the layer just after it is deposited, irrespective of the type of sample. A deeper analysis of the temperature trend was performed using a measuring point, as shown in Fig. 13. This enabled the temperature variation to be evaluated during the deposition. As can be inferred, the temperature trends repeat periodically, where the period is the interlayer time. This can be better observed in the zoom-in plot shown in Fig. 14. As it can be observed, during the

Fig. 10 Fracture surfaces of waterjet cut samples of different thicknesses: **a** 2.5 mm and **b** 3.0 mm
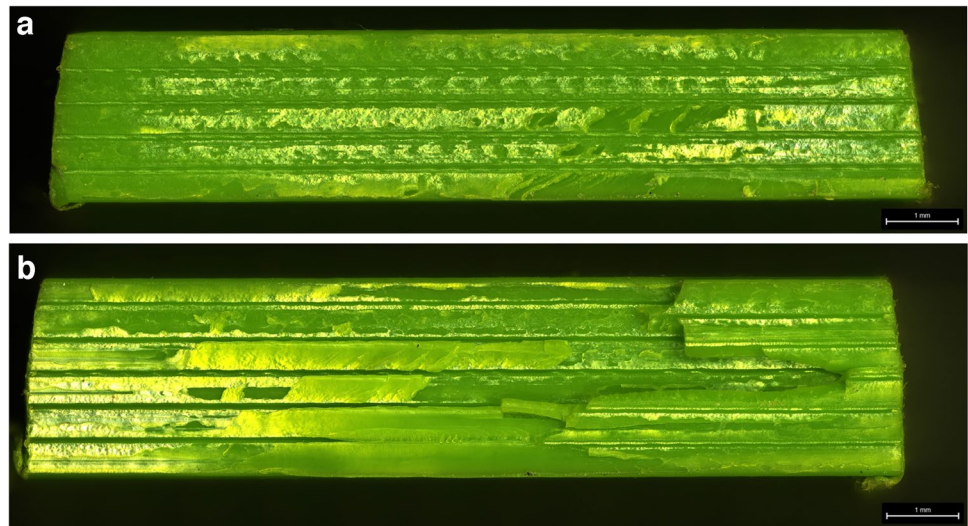

Fig. 11 Cross sections of **a** directly printed and **b** cut samples
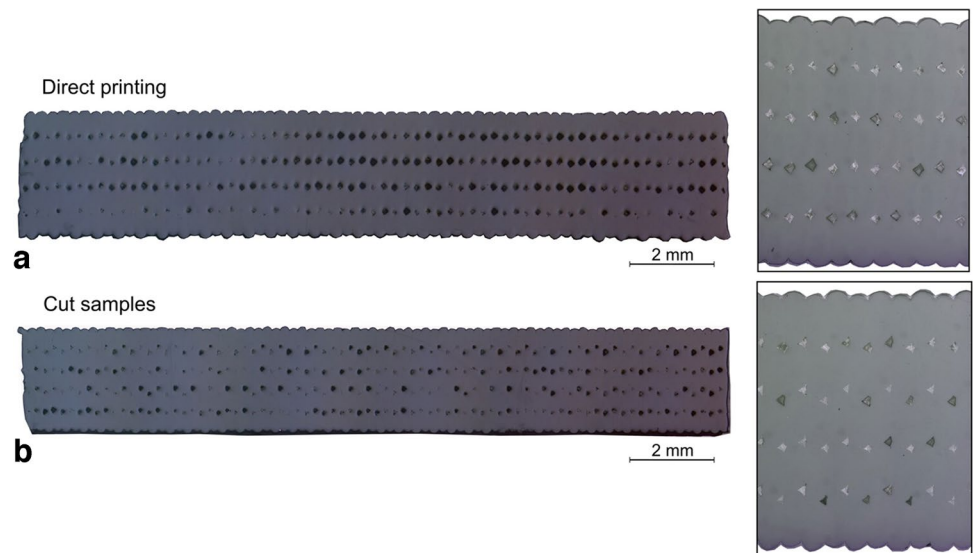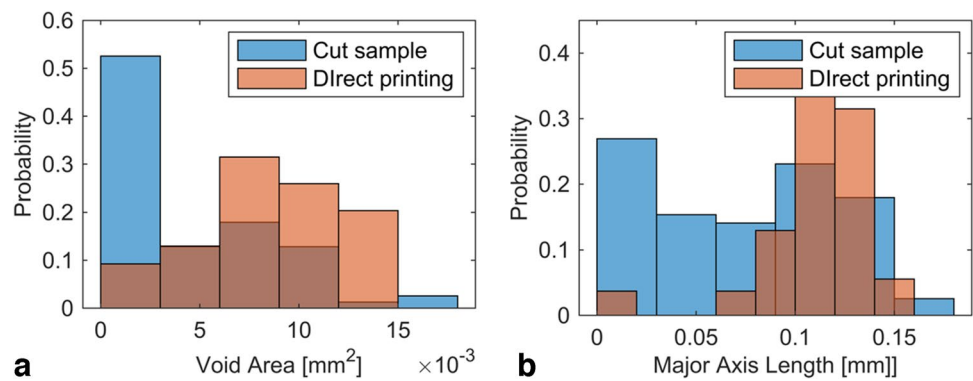

Fig. 12 Dimensional characterization of interlayer voids produced on samples made by direct printing and cutting

depositing of directly printed samples, the temperature of the substrate is higher than that measured in larger components. This is due to the lower interlayer time of 2.5 mm

of thickness (9.3 s) and 3.0 mm of thickness (10.8 s) as compared to the production of the box, whose interlayer time requires 29.9 s. Consequently, when direct samples
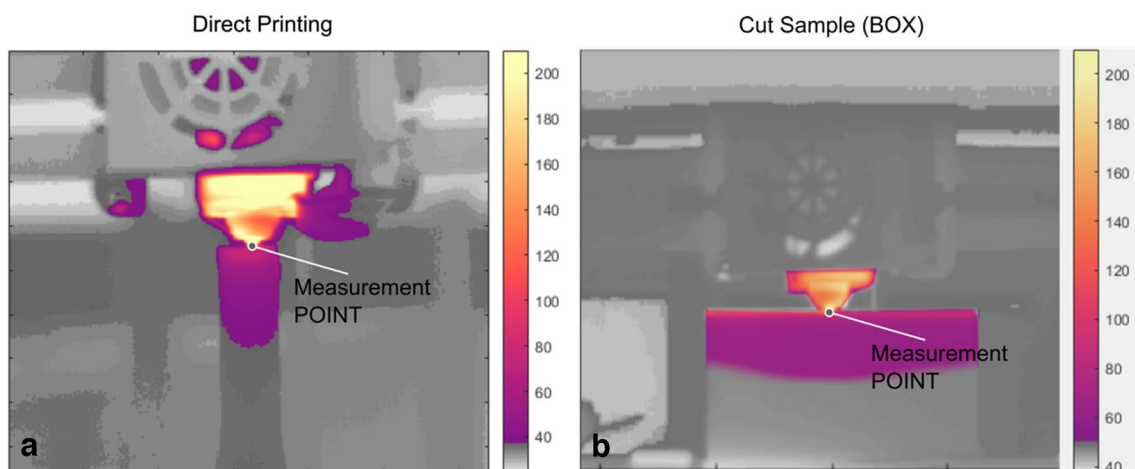
Fig. 13 Infrared pictures acquired during deposition of **a** direct sample printing and **b** box printing for sample cutting

are produced, a higher substrate temperature is faced (125 °C vs. 79 °C), leading to higher intermolecular chain entanglement. This, in turn, enhances the strength of the samples printed directly, leading to an artificially higher strength than samples extracted from a larger component.

4 Discussion

The investigation into the impact of the manufacturing strategy of tensile specimens made by the Material Extrusion process has yielded significant insights. Direct specimen printing has been largely used for the mechanical characterization of MatExt components since its easiness. However, the experimental tests from this study, which also involved tensile specimens cut through abrasive waterjet cutting, shed

light on the significant differences in the mechanical behavior identified by these two. The investigation into the manufacturing strategy's impact on tensile specimens produced by the Material Extrusion process has provided valuable insights. While direct specimen printing has been widely employed for MatExt component mechanical characterization due to its simplicity, this study's experimental tests, including tensile specimens cut via abrasive waterjet, have uncovered significant differences in mechanical behavior between these two approaches.

Directly printed samples exhibited higher tensile strength compared to waterjet-cut samples, attributed to two key phenomena:

1. Enhanced adhesion at side regions: directly printed samples displayed higher adhesion at the side regions, evident from interlayer fractures originating at the sides and the increased irregularity of the fracture surface compared to the smoother central region. This enhanced adhesion was attributed to different deposition conditions at the edge, where tool reversal motions involved deceleration, change of direction, and acceleration (resulting in lower tool speed). This, coupled with a lack of reduction in material flow, led to a higher local material deposition acting as reinforcement, altering the mechanical behavior.

2. Different thermal history: the production of direct samples involved a distinct thermal history compared to the box from which the samples were cut. Variances in interlayer time and convection heat exchanges within the building chamber contributed to this difference. Directly printed samples had interlayer times of 9.3 s (for $t = 2.5$ mm) and 10.8 s (for $t = 3.0$ mm), while the box's interlayer time was nearly triple (29.9 s). Samples cut from the box experienced lower average temperatures, hinder-
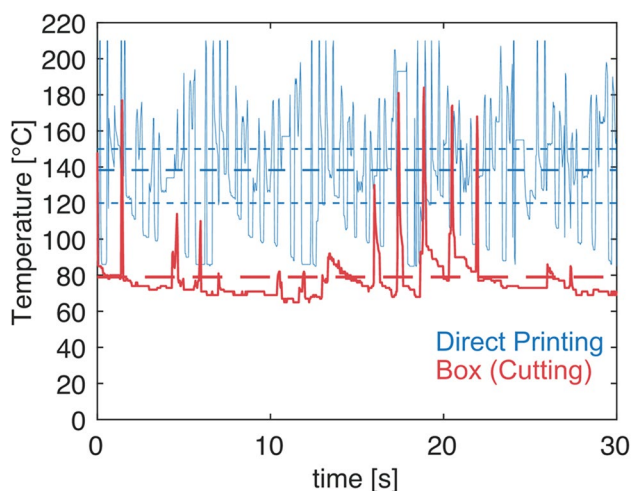

Fig. 14 Thermal history recorded during deposition of direct samples and box

ing prolonged interfilamentous polymer chain entanglement and consequently reducing tensile strength.

The thickness of the samples also exerted a significant, albeit lesser, influence on the components' mechanical behavior. Thicker samples exhibited higher mechanical properties compared to thinner samples, with more pronounced effects on cut samples. In directly printed samples, changes in thickness yielded opposing effects due to increased thermal inertia and interlayer time. For the box, where the interlayer time was consistent, the comparison of mechanical behavior in cut samples highlighted the influence of thermal capacity. Thicker specimens, particularly those cut from the 3.0-mm plate, exhibited higher mechanical behavior due to increased thermal capacity, leading to higher mean temperatures and, consequently, enhanced intermolecular chain entanglement.

Although this investigation focused on PLA, it is plausible to hypothesize that directly printed samples of alternative materials may exhibit analogous artifacts in comparison to cut samples. However, the extent of such artifacts, including both edge effects and variations in thermal history, is likely contingent upon various material properties, deposition parameters, and the specific characteristics of the MEX apparatus employed.

The current study employed fixed deposition conditions, yet certain process parameters such as hotend temperature, cooling rate, and deposition speed could introduce varying degrees of disparity between directly printed and cut samples, given their influence on material viscosity and thermal history.

Therefore, it is conceivable that directly printed samples composed of distinct materials with divergent rheological properties, thermal responses, and crystallization kinetics may exhibit comparable artifacts relative to cut samples; nevertheless, quantifying these differences in material behavior remains necessary. While beyond the scope of the present investigation, a logical progression would entail assessing the impact of alternative printing materials and process parameters on the disparities between directly printed and cut samples.

Furthermore, the reinforcement observed in directly printed samples due to frequent changes in deposition direction presents an opportunity to develop novel deposition strategies aimed at enhancing the mechanical properties and resistance to delamination of MEX components.

This result carries crucial implications for design considerations, emphasizing that different elastic and fracture properties characterize features of varying thickness. Designers should be mindful of different thermal histories in thinner and thicker parts, avoiding thin walls where lower thermal capacity could result in faster cooling and reduced intermolecular entanglement. Careful consideration of these factors is essential for optimizing component design and performance.

5 Conclusions

The study focused on investigating how the manufacturing procedure of tensile specimens made through the Material Extrusion process may alter the mechanical behavior measured during tests. To this end, samples were made by direct printing and extraction (waterjet cutting) from a larger component. Besides, specimens of different thicknesses and according to different types were produced. The findings underscore how critical the manufacturing procedure is since it may significantly alter the mechanical behavior of the sample. To gather deeper insights into such differences, IR thermography and fracture surface analysis were performed. The main results from the research are summarized as follows:

- Even when the deposing parameters directly printed and cut samples were produced using the same process conditions (extrusion temperature, the deposition speed, etc.), the mechanical behavior of the components were strongly influenced by the dimension of the component. Such difference was due to geometrical artifacts and different thermal history. The tensile strength measured through directly printed samples provided an overestimation of the value determined on a sample cut from a larger component (box).
- Directly printed samples involved shorter interlayer time. This led to higher substrate temperature during the deposition. This, in turn, resulted in higher intermolecular entanglement as compared to that achieved on the lager component.
- Direct printing of tensile specimens introduced significant deposition artifacts. These consisted of uneven material flow, which was due to deceleration, reversal of motion, and acceleration in correspondence with the specimens' edges. Such samples were characterized by higher densities at the edges than in the central region. On the other hand, cut samples were not affected by such uneven deposition since the edges were cut out from the samples.
- Directly printed samples showed larger voids than extracted samples. This contributed to altering the Young's modulus measurement.
- The thickness of the specimens also represents a key factor influencing the mechanical behavior measurements. The cut samples of 2.5 mm of thickness were characterized by lower Young's modulus (2.4 GPa) and tensile strength (23.1 MPa) as compared to 3.0 mm (2.8 GPa) and 27.9 MPa, respectively.

- Among ASTM D638 samples, Type V ones provided unreliable results since they failed prematurely during the tests. Even though they were extracted from the same box of cut samples, the tensile strength of these samples (20.9 MPa) was much lower than that observed through the other specimens of Type II. These samples failed at the fillet rather than at the narrow straight section.

Data availability The data supporting this study's findings are available from the corresponding author, Francesco Lambiase, upon reasonable request.

Declarations

Conflict of interest The authors declare no competing interests.

References

1. Calignano F et al (2017) Overview on additive manufacturing technologies. Proc IEEE 105(4):593–612
2. Gibson I, Rosen D, Stucker B, Khorasani A (2021) Materials for additive manufacturing. Addit Manuf Technol 379–428
3. Mohamed OA, Masood SH, Bhowmik JL (2015) Optimization of fused deposition modeling process parameters: a review of current research and future prospects. Adv Manuf 3:42–53
4. Najmon JC, Raeisi S, Tovar A (2019) Review of additive manufacturing technologies and applications in the aerospace industry. Addit Manuf Aerospace Industry 7–31
5. Leal R et al (2017) Additive manufacturing tooling for the automotive industry. Int J Adv Manuf Technol 92:1671–1676
6. Ghomi ER et al (2021) Future of additive manufacturing in healthcare. Curr Opin Biomed Eng 17:100255
7. Bogers M, Hadar R, Bilberg A (2016) Additive manufacturing for consumer-centric business models: implications for supply chains in consumer goods manufacturing. Technol Forecast Soc Chang 102:225–239
8. Velasco-Hogan A, Xu J, Meyers MA (2018) Additive manufacturing as a method to design and optimize bioinspired structures. Adv Mater 30(52):1800940
9. Despeisse, M. and S. Ford. The role of additive manufacturing in improving resource efficiency and sustainability. in Advances in Production Management Systems: Innovative Production Management Towards Sustainable Growth: IFIP WG 5.7 International Conference, APMS 2015, Tokyo, Japan, September 7-9, 2015, Proceedings, Part II 0. 2015. Springer.
10. Plocher J, Panesar A (2019) Review on design and structural optimisation in additive manufacturing: towards next-generation lightweight structures. Mater Des 183:108164
11. Huang R et al (2016) Energy and emissions saving potential of additive manufacturing: the case of lightweight aircraft components. J Clean Prod 135:1559–1570
12. Seharing A, Azman AH, Abdullah S (2020) A review on integration of lightweight gradient lattice structures in additive manufacturing parts. Adv Mech Eng 12(6):1687814020916951
13. Martins RF et al (2021) Structural integrity of polymeric components produced by additive manufacturing (AM)—polymer applications. Polymers 13(24):4420
14. Kobenko S et al (2022) Structural integrity of the aircraft interior spare parts produced by additive manufacturing. Polymers 14(8):1538
15. Cuan-Urquizo E et al (2019) Additive manufacturing and mechanical properties of lattice-curved structures. Rapid Prototyp J 25(5):895–903
16. Holmes M (2019) Additive manufacturing continues composites market growth. Reinf Plast 63(6):296–301
17. Dua R et al (2021) Applications of 3D-printed PEEK via fused filament fabrication: a systematic review. Polymers 13(22):4046
18. Qattawi A, Ablat MA (2017) Design consideration for additive manufacturing: fused deposition modelling. Open J Appl Sci 7(6):291–318
19. Solomon IJ, Sevvel, Gunasekaran J (2021) A review on the various processing parameters in FDM. Mater Today Proc 37:509–514
20. Medellin-Castillo HI, Zaragoza-Siqueiros J (2019) Design and manufacturing strategies for fused deposition modelling in additive manufacturing: a review. Chin J Mech Eng 32(1):1–16
21. Kechagias JD, Zaoutsos S (2023) An investigation of the effects of ironing parameters on the surface and compression properties of material extrusion components utilizing a hybrid-modeling experimental approach. Prog Addit Manuf 1–13. https://doi.org/10.1007/s40964-023-00536-2
22. Kechagias J, Zaoutsos S (2024) Effects of 3D-printing processing parameters on FFF parts' porosity: outlook and trends. Mater Manuf Process:1–11
23. Scipioni SI, Lambiase F (2023) Yielding and post-yielding behavior of FDM parts under compression stress at different strain rates. Int J Adv Manuf Technol 128(3-4):1199–1211
24. Lambiase F, Scipioni SI, Paoletti A (2022) Determination of local density in components made by fused deposition modeling through indentation test. Int J Adv Manuf Technol 122(3):1467–1478
25. Ding H et al (2022) Developing fused deposition modeling additive manufacturing processing strategies for aluminum alloy 7075: sample preparation and metallographic characterization. Materials 15(4):1340
26. Dave HK et al (2021) Effect of multi-infill patterns on tensile behavior of FDM printed parts. J Braz Soc Mech Sci Eng 43(1):23
27. Gordelier TJ et al (2019) Optimising the FDM additive manufacturing process to achieve maximum tensile strength: a state-of-the-art review. Rapid Prototyp J 25(6):953–971
28. Sehhat MH, Mahdianikhotbesara A, Yadegari F (2022) Impact of temperature and material variation on mechanical properties of

parts fabricated with fused deposition modeling (FDM) additive manufacturing. Int J Adv Manuf Technol 120(7-8):4791–4801

29. Gebisa AW, Lemu HG (2019) Influence of 3D printing FDM process parameters on tensile property of ULTEM 9085. Procedia Manuf 30:331–338
30. Pulipaka A et al (2023) Effect of 3D printing process parameters on surface and mechanical properties of FFF-printed PEEK. J Manuf Process 85:368–386
31. Singh J, Goyal KK, Kumar R (2022) Effect of filling percentage and raster style on tensile behavior of FDM produced PLA parts at different build orientation. Mater Today: Proc 63:433–439
32. Naranjo-Lozada J et al (2019) Tensile properties and failure behavior of chopped and continuous carbon fiber composites produced by additive manufacturing. Addit Manuf 26:227–241
33. Maqsood N, Rimašauskas M (2021) Delamination observation occurred during the flexural bending in additively manufactured PLA-short carbon fiber filament reinforced with continuous carbon fiber composite. Results Eng 11:100246
34. Islam M, Prabhakar (2017) Interlaminar strengthening of multidirectional laminates using polymer additive manufacturing. Mater Des 133:332–339
35. Jin Z, Zhang Z, Gu GX (2020) Automated real-time detection and prediction of interlayer imperfections in additive manufacturing processes using artificial intelligence. Adv Intell Syst 2(1):1900130
36. Roy M, Wodo O (2020) Data-driven modeling of thermal history in additive manufacturing. Addit Manuf 32:101017
37. Roy M et al (2019) Prediction and experimental validation of part thermal history in the fused filament fabrication additive manufacturing process. J Manuf Sci Eng 141(12):121001
38. Lee A et al (2022) Effect of temperature history during additive manufacturing on crystalline morphology of PEEK. Adv Ind Manuf Eng 4:100085
39. Deshpande A et al (2019) Interlayer thermal history modification for interface strength in fused filament fabricated parts. Prog Addit Manuf 4:63–70
40. Scipioni SI, Lambiase F (2023) Error introduced by direct 3D printing of compression samples of PLA made by FDM process. Int J Adv Manuf Technol 129(9–10):4355–4368
41. d6.5d, ASTM D 638. Standard test method for tensile properties of plastics. 2000.